

1      **A direct comparison between field-measured**

2      **and sensor-based estimates of soil carbon**

3      **dioxide flux across six National Ecological**

4      **Observatory Network sites enabled by the**

5      **neonSoilFluxR packageneonSoilFlux: An R**

6      **Package for Continuous Sensor-Based**

7      **Estimation of Soil CO<sub>2</sub> Fluxes**

8                John Zobitz<sup>1</sup>      Ed Edward Ayres<sup>2</sup>      Zoey Werbin<sup>3</sup>

9                Ridwan Abdi<sup>1</sup>      Natalie Ashburner-Wright<sup>4</sup>      Lillian Brown<sup>4</sup>

10          Ryan Frink-Sobierajski<sup>4</sup>      Lajntxiag Lee<sup>1</sup>      Dijonë Mehmeti<sup>1</sup>

11          Christina Tran<sup>4</sup>      Ly Xiong<sup>1</sup>      Naupaka Zimmerman<sup>4,5</sup>

12      <sup>1</sup> Augsburg University, 2211 Riverside Avenue, Minneapolis, MN 55454

13      <sup>2</sup> National Ecological Observatory Network, Battelle, 1685 38th Street, Suite 100, Boulder, CO  
14      80301

<sup>15</sup> <sup>3</sup> Boston University, 5 Cummington Street, Boston, MA 02215

<sup>16</sup> <sup>4</sup> University of San Francisco, 2130 Fulton Street, San Francisco, CA 94117

<sup>17</sup> <sup>5</sup> University of Kansas, 1450 Jayhawk Boulevard, Lawrence, KS 66045

## <sup>18</sup> **Acknowledgments**

<sup>19</sup> JZ acknowledges Kathleen O'Rourke for code development. NZ thanks technical staff at  
<sup>20</sup> USF for support with field gear assembly and shipping. We thank the NEON field staff and  
<sup>21</sup> assignable assets teams for facilitating each of the six NEON site visits. We are grateful to  
<sup>22</sup> LI-COR technical staff for helpful discussions about optimal soil chamber sampling methods.

<sup>23</sup> This work was supported by NSF DEB grant #2017829 awarded to JZ, and NSF DEB grant  
<sup>24</sup> #2017860 awarded to NZ. This material is based in part upon work supported by the National  
<sup>25</sup> Ecological Observatory Network (NEON), a program sponsored by the U.S. National Science  
<sup>26</sup> Foundation (NSF) and operated under cooperative agreement by Battelle. We also thank the  
<sup>27</sup> reviewers and subject editor for their constructive feedback.

## <sup>28</sup> **Conflict of Interest Statements**

<sup>29</sup> None of the authors have a financial, personal, or professional conflict of interest related to this  
<sup>30</sup> work.

## <sup>31</sup> **Author Contributions**

<sup>32</sup> Conceptualization: JZ, NZ; Methodology: EA, JZ, NZ; Software: JZ, NZ, ZW, E A, DM, RA,  
<sup>33</sup> LX, LL; Validation: JZ, NZ; Formal Analysis: JZ, NZ, DM, RA, LX, LL; Investigation: JZ, NZ,

<sup>34</sup> RF-S, CT, NA-W, LB; Resources: JZ, NZ; Data curation: JZ, NZ, DM, LX; Writing – original  
<sup>35</sup> draft: JZ, NZ; Writing – review and editing: JZ, NZ, ZW, EA, CT, DM, LX,; Visualization: JZ,  
<sup>36</sup> NZ, DM, RA, LX; Supervision: JZ; NZ; Project Administration: JZ; NZ; Funding Acquisition:  
<sup>37</sup> JZ; NZ

## <sup>38</sup> **Data Availability**

<sup>39</sup> ~~Data available~~ Anonymous field-collected data, neonSoilFlux calculated outputs, and  
<sup>40</sup> manuscript-generating code for peer review are provided as supplemental files. All will  
<sup>41</sup> be made available via Zenodo prior to publicly available on Zenodo with a DOI upon  
<sup>42</sup> publication.

43 **1 Abstract**

44 A key component of constraining the uncertainty Accurate quantification of soil carbon fluxes  
45 is essential to reduce uncertainty in estimates of the terrestrial carbon sink is quantification  
46 of terrestrial soil carbon fluxes, which vary across time and ecosystem type. One method for  
47 the estimation of these fluxes and their associated uncertainties is the flux gradient method,  
48 which can be calculated via a variety of existing approaches. Robust estimation of. However,  
49 these fluxes vary over time and across ecosystem types and so it can be difficult to estimate  
50 them accurately across large scales. The flux gradient method estimates soil carbon fluxes on a  
51 sub-daily level requires using co-located measurements of soil CO<sub>2</sub> concentration, water content,  
52 temperature, and other environmental measurements and soil temperature, soil moisture, and  
53 other soil properties. These data are publicly available from the The National Ecologi-  
54 cal Observatory Network at sites spanning a range of (NEON) provides such data across  
55 20 different ecoel climatic domains across the continental United States ecoclimatic domains  
56 spanning the continental U.S., Puerto Rico, Alaska, and Hawai'i. We present an R soft-  
57 ware package (`neonSoilFlux`) that acquires NEON soil environmental data and computes  
58 soil carbon flux at a half-hourly time step at a user-specified NEON site and month in a tidy  
59 data format. To validate to compute half-hourly soil carbon fluxes for each soil replicate  
60 plot at a given terrestrial NEON site. To assess the computed fluxes, we visited six focal  
61 NEON sites and measured soil carbon fluxes using a closed-dynamic chamber approach.  
62 The validation confirmed that a primary challenge in reducing soil carbon flux uncertainty is  
63 correctly characterizing diffusivity and soil water content across the soil profile. Outputs from  
64 the `neonSoilFlux` package showed agreement with measured fluxes ( $R^2$  between measured  
65 and `neonSoilFlux` outputs ranging from 0.04 to 0.81 depending on calculation method used);  
66 measured outputs generally fell within the range of calculated uncertainties from the gradient  
67 method. Calculated fluxes from `neonSoilFlux` aggregated to the daily scale exhibited expected

68 site-specific seasonal patterns. While the flux gradient method is broadly effective, its accuracy  
69 is highly sensitive to site-specific inputs, including the extent to which gap-filling techniques  
70 are used to interpolate missing sensor data and to estimates of soil diffusivity and moisture  
71 content. Future refinement and validation of `neonSoilFlux` outputs can contribute to existing  
72 databases of soil carbon flux measurements, providing near real-time estimates of a critical  
73 component of the terrestrial carbon cycle.

## 74 **1.1 Keywords**

75 Soil carbon, carbon dioxide, flux gradient, carbon cycle, field validation, soil respiration,  
76 ecosystem variability, diffusion

## 77 **2 Data for peer review**

78 Anonymous ~~data and field-collected data, `neonSoilFlux` calculated outputs, and~~  
79 ~~manuscript-generating~~ code for peer review ~~is available here: [LINK](#)~~ are provided as  
80 supplemental files. All will be made publicly available on Zenodo with a DOI upon  
81 publication.

## 82 **3 Introduction**

83 Soils contain the planet's largest reservoir of terrestrial carbon (Jobbágy & Jackson, 2000). A  
84 critical component of this reservoir is soil organic matter, the accumulation of which is influenced  
85 by biotic factors such as above-ground plant inputs (Jackson et al., 2017). These inputs in  
86 turn are influenced by environmental factors such as growing season length, temperature, and

moisture (Desai et al., 2022), which also affect the breakdown of soil organic matter and its return to the atmosphere. Across heterogeneous terrestrial landscapes, the interplay between these biotic and abiotic factors influence the size of the soil contribution to the terrestrial carbon sink (Friedlingstein et al., 2023~~2025~~). However, the heterogeneity of these processes across diverse ecosystems in the context of rapid environmental change leads to large uncertainty ~~in about~~ the magnitude of this sink in the future, and thus ~~there remains~~ a pressing need to quantify changes in soil carbon pools and fluxes across scales.

Ecological observation networks such as the United States' National Ecological Observatory Network (NEON) and others (e.g. the globally-distributed FLUXNET or the European Integrated Carbon Observation System) present a significant advancement in the nearly continuous observation of biogeochemical processes at the continental scale. Notably, at 47 terrestrial sites across the continental United States that span 20 ecoclimatic domains, NEON provides half-hourly measurements of soil CO<sub>2</sub> concentration, temperature, and moisture at different vertical depths. Each of these NEON sites also encompasses measurements of the cumulative sum of all ecosystem carbon fluxes in an airshed using the eddy covariance technique (Baldocchi, 2014). Soil observations provided by NEON are on the same timescale and standardized with eddy covariance measurements from FLUXNET. These types of nearly continuous observational data (NEON and FLUXNET) can be used to reconcile differences between model-derived or data-estimated components of ecosystem carbon flux (Jian et al., 2022; Luo et al., 2011; Phillips et al., 2017; J. Shao et al., 2015; P. Shao et al., 2013; Sihi et al., 2016).

Estimated or observed soil carbon fluxes are a key metric for understanding change in soil carbon pools over time (Bond-Lamberty et al., 2024). A soil carbon flux to the atmosphere ( $F_S$ , units  $\mu\text{mol m}^{-2} \text{s}^{-1}$ ), represents the aggregate process of transfer of soil CO<sub>2</sub> to the atmosphere from physical and biological processes (e.g. diffusion and respiration). Soil carbon fluxes can be assumed to encompass soil carbon respiration from autotrophic or heterotrophic sources

112 (Davidson et al., 2006) ~~, typically assumed to be static across the soil biome~~ and modeled with  
113 a exponential  $Q_{10}$  paradigm (Bond-Lamberty et al., 2004; Chen & Tian, 2005; Hamdi et al.,  
114 2013).

115 One common method by which  $F_S$  is measured in the field is through the use of soil chambers  
116 in a closed, well-mixed system (Norman et al., 1997) with headspace trace gas concentra-  
117 tions measured with an infrared gas analyzer (IRGA).  $F_S$  can also be estimated from soil  
118  $\text{CO}_2$  measurements at different depths in the soil using the flux-gradient method (Maier &  
119 Schack-Kirchner, 2014). ~~This method is Closed-chamber IRGA measurements, while being the~~  
120 ~~most common method, require either frequent in-person site visits or expensive and fragile~~  
121 ~~automated systems. The potential of the gradient method is that fluxes can be estimated~~  
122 ~~from continuous data recorded by robust solid-state sensors. The flux-gradient method is~~ an  
123 approach that uses conservation of mass to calculate flux at a vertical soil depth  $z$  at steady state  
124 by applying Fick's law of diffusion. A simplifying assumption for the flux-gradient method is  
125 that there is no mass transfer in the other spatial dimensions  $x$  and  $y$  (Maier & Schack-Kirchner,  
126 2014). The diffusivity profile, a key component of this calculation, varies across the soil depth  
127 as a function of soil temperature, soil volumetric water content, atmospheric air pressure, and  
128 soil bulk density (Millington & Shearer, 1971; Moldrup et al., 1999; Sallam et al., 1984).

129 Databases such as the Soil Respiration Database (SRDB) or the Continuous Soil Respiration  
130 Database (COSORE) add to the growing network of resources for making collected observations  
131 of soil fluxes available to other ~~workers~~researchers (Bond-Lamberty, 2018; Bond-Lamberty et  
132 al., 2020; Bond-Lamberty & Thomson, 2010; Jian et al., 2021; Jiang et al., 2024). However,  
133 these databases currently encompass primarily direct soil measurements of fluxes (i.e. those  
134 using methods like the closed-chamber method described above). Currently, NEON provides  
135 all measurements to calculate  $F_S$  from Fick's law, but soil flux as a derived data product was  
136 descoped from the initial network launch due to budget constraints (Berenbaum et al., 2015).

<sup>137</sup> Deriving estimates of  $F_S$  using continuous sensor data across NEON sites thus ~~represents~~  
<sup>138</sup> remains a high priority.

<sup>139</sup> This study describes an R software package, `neonSoilFlux`, that ~~can be used to derive~~  
<sup>140</sup> computes a standardized estimate of  $F_S$  at all terrestrial NEON sites ~~. After calculating~~  
<sup>141</sup> ~~these flux estimates, we then validated them against using the flux-gradient method. Using~~  
<sup>142</sup> direct chamber-based field observations of soil carbon dioxide flux from a subset of terrestrial  
<sup>143</sup> NEON sites spanning six states, we provide a direct validation of  $F_S$  from `neonSoilFlux`.

<sup>144</sup> Key objectives of this study are to:

- <sup>145</sup> 1. Apply the flux-gradient method to estimate soil CO<sub>2</sub> flux from continuous sensor mea-  
<sup>146</sup> surements across six NEON sites.
- <sup>147</sup> 2. Benchmark estimated soil carbon fluxes against field measurements (e.g. direct chamber  
<sup>148</sup> measurements of soil flux).
- <sup>149</sup> 3. Identify sources of error in the flux-gradient approach across diverse sites in order to  
<sup>150</sup> guide future work.

## <sup>151</sup> 4 Materials and Methods

### <sup>152</sup> 4.1 Field methods

#### <sup>153</sup> 4.1.1 Focal NEON Sites

<sup>154</sup> In order to acquire field data to validate model predictions of flux, we selected six terrestrial  
<sup>155</sup> NEON sites for analysis. We conducted roughly week-long field measurement campaigns at  
<sup>156</sup> these sites, which span a range of environmental gradients and terrestrial domains (Table 1).

157 SJER, SRER, and WREF were visited during May and June of 2022, and WOOD, KONZ,  
158 and UNDE during May and June of 2024.

159 ~~Over the course of two field campaigns in 2022 and 2024, we conducted week-long visits at~~  
160 ~~each site. In consultation with NEON field staff, we first selected a specific plot in the soil~~  
161 ~~sampling array to maximize the concurrent availability of sensor data.~~

162 **4.1.2 Soil collar placement**

163 Either one (2022 sampling campaign) or two (2024 sampling campaign) PVC soil collars (20.1  
164 cm inside diameter) were installed in close proximity to the permanent NEON soil sensors  
165 at each site (Figure 1). ~~The soil plot where measurements were taken~~ As instruments in the  
166 ~~NEON soil sensor arrays can occasionally break down or stop working, the specific soil plot~~  
167 ~~where we made measurements~~ was chosen at each site in consultation with NEON staff to  
168 maximize likelihood of quality soil sensor measurements during the duration of the IRGA  
169 measurements. ~~The plot selected~~ at each site (~~out of the 5 in each replicate array at each site~~)  
170 ~~are presented in the last column of Table 1~~. After installation, collar(s) were left to equilibrate  
171 for approximately 24 hours prior to any measurements being taken.

172 **4.1.3 Infrared gas analyzer measurements of soil CO<sub>2</sub> flux**

173 In 2022, we then made measurements of flux on an hourly interval for 8 hours each day.  
174 Measurements were taken from roughly 8 am to 4 pm, with the time interval selected to  
175 capture the majority of the diurnal gradient of soil temperature each day. These measurements  
176 were made using a LI-6800 infrared gas analyzer instrument (LI-COR Environmental, Lincoln,  
177 NE) fitted with a soil chamber attachment (attachment 6800-09). In 2024, we again used the  
178 same LI-6800 instrument, but made half-hourly measurements over an approximately 8 hour

179 period. In addition, [in 2024](#) we also installed a second collar and used a second instrument, an  
180 LI-870 CO<sub>2</sub> IRGA, connected to an automated robotic chamber (LI-COR chamber 8200-104)  
181 controlled by an LI-8250 multiplexer ~~✓~~ to make automated measurements. The multiplexer was  
182 configured to take half-hourly measurements 24 hours a day for the duration of our sampling  
183 bout at each site. Each instrument was paired with a soil temperature and moisture probe  
184 (Stevens HydraProbe, Stevens Water, Portland, OR) that was used to make soil temperature  
185 and moisture measurements concurrent with the CO<sub>2</sub> flux measurements. Chamber volumes  
186 were set by measuring collar offsets at each site. System checks were conducted daily for the  
187 LI-6800 and weekly for the LI-8250. Instruments were factory calibrated before each field  
188 season.

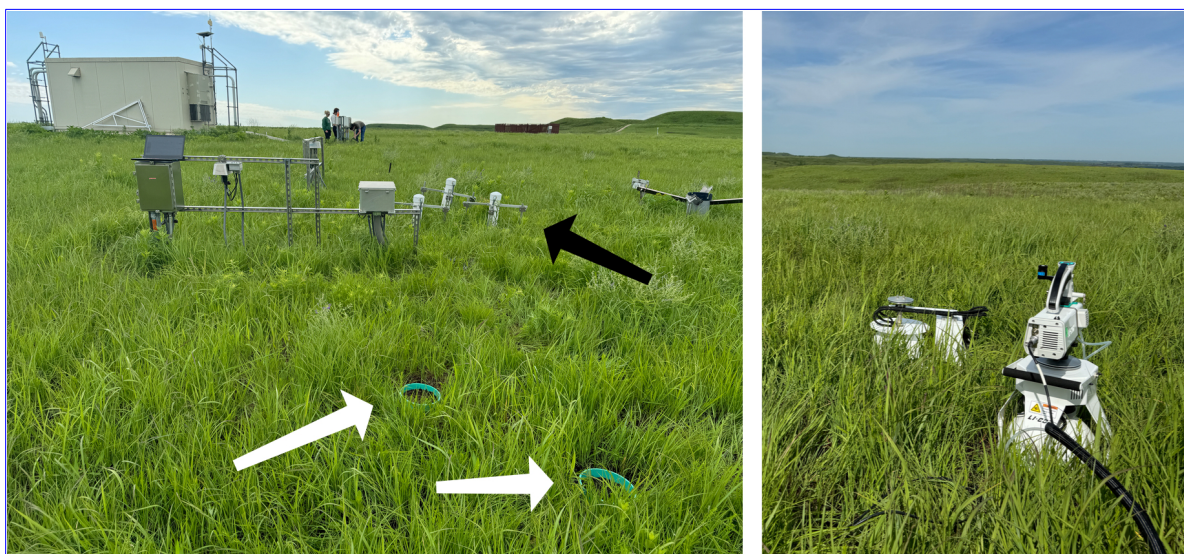


Figure 1: Spatial layout of field sampling using a closed-dynamic chamber setup at a representative NEON site (KONZ). Left image shows collars (white arrows) and permanent soil sensor installation (black arrow) and right image shows the LI-6800 (foreground) and LI-8200-104 (background) instruments placed on the collars.

g of NEON sites studied for field work and analysis. Site refers to NEON site Santa Rita Experimental Range (SRER), San Joaquin Experimental Range (SJER), Wind River Experimental Forest (WREF), Chase Lake National Wildlife Refuge (WOOD), Konza Prairie Biological Station (KONZ), and the University of Notre Dame Environmental Research Center (UNDE). Location is reported in decimal degrees of latitude and longitude. Other abbreviations include Mean Annual Temperature (MAT);  $T_S$ : average soil temperature during field measurements; SWC: average soil water content during field measurements. Soil plot Dates refer to field measurement dates for each site. Plot refers to the particular location in the soil array (denoted as HOR by NEON) where field measurements were made.

Site (NEON site ID)	Location	Ecosystem type	Mean annual	Mean annual	Field measurement	Soil plot Plot	
			MAT	$T_S$ ( $^{\circ}$ C)	MAP		
Santa Rita Experimental Range (SRER)	31.91068, -110.83549	Shrubland	19.3 °C	47.6 °C	346 mm	4.0%	004 29-May 2024-01 June 2024 May 29- June 1 2022
San Joaquin Experimental Range (SJER)	37.10878, -119.73228	Oak woodland	16.4 °C	41.7 °C	540 mm	1.2%	005 01-June 2022-04 June 1-4 2022
Wind River Experimental Forest (WREF)	45.82049, -121.95191	Evergreen forest	9.2 °C	15.3 °C	2225 mm	27.2%	001 07-June 2022-09 June 7-9 2022
Chase Lake National Wildlife Refuge (WOOD)	47.1282, -99.241334	Restored prairie grassland	4.9 °C	14.9 °C	495 mm	14.9%	001 03-June 2024-09 June 3-9 2024
Konza Prairie Biological Station (KONZ)	39.100774, -96.563075	Tallgrass prairie	12.4 °C	23.4 °C	870 mm	23.4%	001 29-May May 29- June 1 2024 -01-June 2024

g of NEON sites studied for field work and analysis. Site refers to NEON site Santa Rita Experimental Range (SRER), San Joaquin Experimental Range (SJER), Wind River Experimental Forest (WREF), Chase Lake National Wildlife Refuge (WOOD), Konza Prairie Biological Station (KONZ), and the University of Notre Dame Environmental Research Center (UNDE). Location is reported in decimal degrees of latitude and longitude. Other abbreviations include Mean Annual Temperature (MAT);  $\overline{T}_S$ : average soil temperature during field measurements; SWC: average soil water content during field measurements. Soil plot Dates refer to field measurement dates for each site. Plot refers to the particular location in the soil array (denoted as HOR by NEON) where field measurements were made.

Site (NEON site ID)	Location	Ecosystem type	Mean annual temperature (MAT)	Mean annual precipitation (MAP)	Mean SWC (%)	Field measurement dates	Soil plot Plot
University of Notre Dame Environmental Research Center (UNDE)	46.23391, -89.537254	Deciduous forest	4.3 °C	13.0 °C	802 mm	13.0% 22-May 2024-25	004 May 22-25 2024

#### 189 4.1.4 Post-collection processing of field data

190 We used LI-COR SoilFluxPro software (v 5.3.1) to assess the data after collection and to  
 191 inform sampling parameters. We checked appropriateness of dead band and measurement  
 192 durations using built-in evaluation tools. Based on this, the deadband period was set for  
 193 30-40 seconds, depending on the site, and the measurement duration was 180 seconds with a  
 194 30 second pre-purge and a 30 second post-purge at most sites, and a 90 see-second pre- and  
 195 post-purge at sites with higher humidity due to recent precipitation events. We also assessed  
 196 the  $R^2$  of linear and exponential model fits to measured CO<sub>2</sub> to verify measurement quality.

197 **4.2 neonSoilFlux R package**

198 We developed an R package ([called](#) `neonSoilFlux` ; [LINK TO BE ADDED AFTER PEER  
REVIEW](#)(Zobitz et al., 2024) to compute half-hourly soil carbon fluxes and uncertainties from  
199 NEON data. The objective of the `neonSoilFlux` package is a unified workflow (Figure 2) for  
200 soil data acquisition and analysis that supplements the existing [neonUtilities](#) data acquisition  
201 R package `neonUtilities` ([LINK TO BE ADDED AFTER PEER REVIEW](#)(Lunch et al.,  
202 [2025](#)).

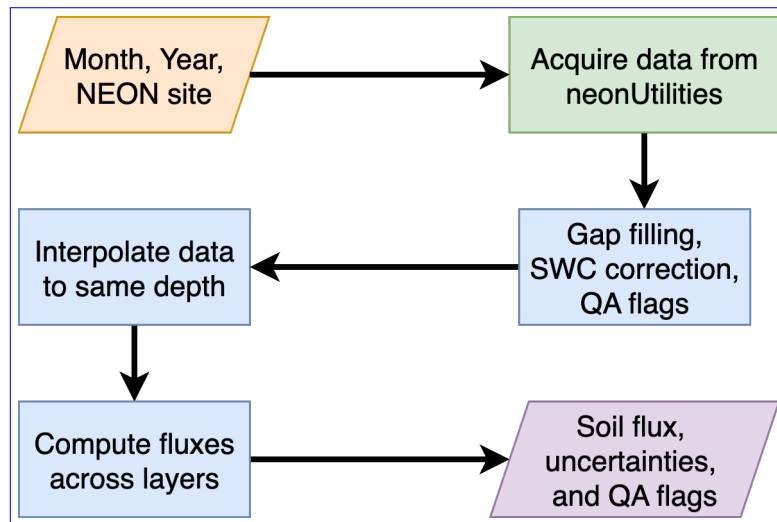


Figure 2: Diagram of `neonSoilFlux` R package. For a given month, year, and NEON site (orange parallelogram), the package acquires all relevant data to compute  $F_S$  using the `neonUtilities` R package (green rectangle). Data are gap-filled according to reported QA flags and [adjusted for changes in soil water content \(SWC\) calibration coefficients, then](#) interpolated to the same measurement depth before computing the soil flux, uncertainties, and final QA flags (blue rectangles). The package reports the associated soil flux, uncertainties, and quality assurance (QA) flags for the user (purple parallelogram).

204 At a given NEON [observation site](#) there are five replicate soil plots, each with measurements  
205 of soil CO<sub>2</sub> concentration, soil temperature, and soil moisture at different depths (Figure 3).  
206 The `neonSoilFlux` package acquires measured soil [water content](#) [CO<sub>2</sub> concentration](#) (National

207 Ecological Observatory Network (NEON), [2024e](#)[2024b](#)), soil ~~CO<sub>2</sub> concentration~~ temperature  
 208 (National Ecological Observatory Network (NEON), [2024b](#)), ~~barometric pressure from the~~  
 209 ~~nearby tower~~[2024d](#)), ~~soil water content~~ (National Ecological Observatory Network (NEON),  
 210 [2024a](#)), ~~soil temperature~~[2024e](#)), ~~barometric pressure from the nearby tower~~ (National Eco-  
 211 logical Observatory Network (NEON), [2024d](#)[2024a](#)), and soil properties (e.g. bulk density)  
 212 (National Ecological Observatory Network (NEON), 2024c) [from a range of different NEON](#)  
 213 [data products](#). The static soil properties were collected [by NEON staff](#) from a nearby soil pit  
 214 during [initial](#) site characterization and are assumed to be constant at each site. [A soil flux](#)  
 215 [calculation is computed at each replicate soil plot.](#)

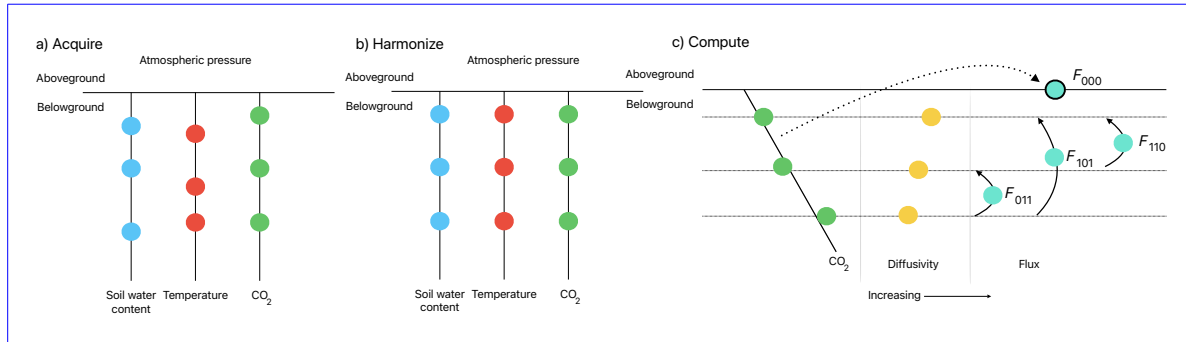


Figure 3: Model diagram [for](#) [of](#) the data workflow for the `neonSoilFlux` R package. a) Acquire: Data are obtained [from](#) [for](#) a given NEON location and horizontal sensor location, which includes soil water content, soil temperature, CO<sub>2</sub> concentration, and atmospheric pressure. All data are screened for quality assurance; if gap-filling of missing data occurs, it is flagged for the user. b) [Harmonize](#): Any belowground data are then harmonized to the same depth as CO<sub>2</sub> concentrations using linear regression. c) [Compute](#): The flux across a given depth is computed via Fick's law, denoted with  $F_{ijk}$ , where  $i$ ,  $j$ , or  $k$  are either 0 or 1 denoting the layers the flux is computed across ( $i$  = closest to surface,  $k$  = deepest).  $F_{000}$  represents a flux estimate where the gradient  $dC/dz$  is the slope of a linear regression of CO<sub>2</sub> with depth.

216 The workflow to compute a value of  $F_S$  with `neonSoilFlux` consists of three primary steps,  
 217 illustrated in Figure 3. First, NEON data are acquired for a given site and month via the  
 218 `neonUtilities` R package (yellow parallelogram and green rectangle in Figure 2 and Panel  
 219 a in Figure 3). Acquired environmental data can be exported to a comma separated value

220 file for additional analysis. Quality assurance (QA) flags are reported as an indicator variable.  
221 Since the calibration coefficients on the soil water content sensors have changed over time  
222 (National Ecological Observatory Network (NEON), 2024e), raw sensor measurements were  
223 back-calculated and soil-specific calibrations were applied following Ayres et al. (2024) to  
224 generate a consistent time series at each measurement location.

225 The second step is harmonizing the data to compute soil fluxes across soil layers. This  
226 step consists of three different actions (blue rectangles in Figure 2 and Panel b in Figure 3).  
227 If a given observation by NEON is reported as not passing a quality assurance check, we  
228 applied a gap filling method to replace that measurement with its monthly mean at that same  
229 depth (Section 4.2.1). Belowground measurements of soil water and soil temperature are then  
230 interpolated to the same depth as soil CO<sub>2</sub> measurements. The diffusivity (Section 4.2.2) and  
231 soil flux across different soil layers (Section 4.2.3) are then computed.

232 The third and final step is computing a surface soil flux through extrapolation to the surface  
233 (purple parallelogram in Figure 2 and Panel c in Figure 3). Uncertainty on a soil flux  
234 measurement is computed through quadrature. An aggregate quality assurance (QA) flag for  
235 each environmental measurement is also reported, representing if any gap-filled measurements  
236 were used in the computation of a soil flux. Within the soil flux-gradient method, several  
237 different approaches can be used to derive a surface flux (Maier & Schack-Kirchner, 2014); the  
238 `neonSoilFlux` package reports four different possible values for soil surface flux (Section 4.2.3)  
239 for each of two different methods of diffusivity estimation, for a total of eight estimates of  
240 flux.

241 **4.2.1 Gap-filling routine**

242 NEON reports QA flags as a binary value for a given binary values for each measurement  
243 and half-hourly time interval. We replaced any flagged measurements at a location's spatial  
244 interval. For a given half-hour, if any input variable (soil CO<sub>2</sub> concentration, soil temperature,  
245 or soil moisture) at depth  $z$  is flagged, computation of  $F_S$  is not possible. To address this,  
246 flagged measurements and their uncertainties were replaced with a bootstrapped sample of  
247 the monthly mean for all un-flagged measurements for that month. These measurements are  
248 represented by the vector monthly mean ( $\bar{m}$ ) and monthly standard deviation ( $\bar{s}$ ) (Efron &  
249 Tibshirani, 1994).

250 For each month, depth  $z$ , and variable, we computed bootstrapped estimates of  $\bar{m}$  and  $\bar{s}$  from  
251 the vectors of unflagged measurements ( $\mathbf{m}$ , standard errors), reported standard errors ( $\sigma$ ), and  
252 the 95% confidence interval (the so-called expanded uncertainty,  $\epsilon$ , or expanded uncertainty;  
253 Farrance & Frenkel (2012))  $\epsilon$ . All of these vectors have length  $M$ . We have that  $\vec{\sigma}_i \leq \vec{c}_i$ . We  
254 define the bias as  $\vec{b} = \sqrt{\epsilon^2 - \sigma^2}$ , which quantifies the spread  
255 of uncertainty in a given period and is incorporated into  $\bar{m}$ .

256 We generate a vector of bootstrap samples of the distribution of the monthly mean  $\bar{m}$  and  
257 monthly standard error  $\bar{\sigma}$  the following ways:

258 Randomly sample from the uncertainty and bias independently:  $\sigma_j$  and the bias  $\mathbf{b}_k$  (not  
259 necessarily the same sample). Generate From these, 5000 bootstrap samples were generated  
260 for  $\mathbf{m}$ ,  $\sigma$ , and  $\mathbf{b}$ . For each sample ( $m_k, b_k, \sigma_k$ ), we generated a vector  $\mathbf{n}$  of length  $N$ , where  
261  $n_i$  is a random sample (length  $N = 5000$ ) by drawing from a normal distribution with mean  
262  $m_i - m_k + b_k$  and standard deviation  $\sigma_j$ . Since  $M < N$ , values from  $\mathbf{m}$  will be reused. With  
263 these  $N$  random samples,  $\bar{y}_i = \vec{x} + \vec{b}_k$  and  $s_i$  is the sample standard deviation of  $\vec{x}$ . We expect  
264 that  $s_i \approx \sigma_j$ . The reported monthly  $\sigma_k$ . The sample mean and standard deviation are then

265 computed  $\bar{y}$  and  $\bar{s}$ . Measurements and uncertainties that did not pass the QA check are then  
266 substituted with  $\bar{y}$  and were then computed from  $n$ . The resulting distributions of sample  
267 means and sample standard deviations provided the bootstrapped monthly mean ( $\bar{m}$ ) and  
268 standard error ( $\bar{s}$ ) respectively.

269 This gap-filling method described here provides a consistent approach for each  
270 data stream, however we recognize that other gap-filling alternatives may be warranted for  
271 longer-term treatment across all data streams. However, alternative approaches may be better  
272 suited for longer gaps (e.g. such as correlations with other NEON measurement levels and/or  
273 soil plots), or measurement specific gap-filling routines or for variable-specific conditions. We  
274 discuss the effect of gap-filling on our measurements results in Section 6.6.1.

#### 275 4.2.2 Soil diffusivity

276 Soil diffusivity  $D_a$  at a given measurement depth is the product of the diffusivity in free air  
277  $D_{a,0}$  ( $\text{m}^2 \text{ s}^{-1}$ ) and the tortuosity  $\xi$  (no units) (Millington & Shearer, 1971).

278 We compute  $D_{a,0}$  with Equation 1:

$$D_{a,0} = 0.0000147 \cdot \left( \frac{T_i + 273.15}{293.15} \right)^{1.75} \cdot \left( \frac{P}{101.3} \right) \quad (1)$$

279 where  $T_i$  is soil temperature ( $^\circ\text{C}$ ) at depth  $i$  (National Ecological Observatory Network (NEON),  
280 2024d) and  $P$  surface barometric pressure (kPa) (National Ecological Observatory Network  
281 (NEON), 2024a).

282 Previous studies by Sallam et al. (1984) and Tang et al. (2003) demonstrated the sensitivity  
283 of modeled  $F_S$  depending on the tortuosity model used to compute

284 diffusivity. At low soil water content, the choice of ~~tortuosity model may lead to order-of~~  
285 ~~magnitude~~ tortuosity model can lead to order-of-magnitude differences in  $D_a$ , which in turn  
286 affect modeled  $F_S$ . The `neonSoilFlux` package ~~uses two different models for currently includes~~  
287 ~~two approaches to calculate~~  $\xi$ , representing the ~~extremes~~ range of tortuosity behavior reported  
288 in Sallam et al. (1984).

289 The first approach ~~uses is~~ the Millington-Quirk model ~~for diffusivity, Equation 2~~ (Millington &  
290 Shearer, 1971), ~~in which tortuosity depends on both porosity and soil water content~~:

$$\xi = \frac{(\phi - SWC_i)^{10/3}}{\phi^2} \quad (2)$$

291 In Equation 2,  $SWC$  is the soil water content at depth  $i$  (National Ecological Observatory  
292 Network (NEON), 2024e) and  $\phi$  is the porosity (~~Equation 3~~), which in turn is a function of soil  
293 physical properties (National Ecological Observatory Network (NEON), 2024c):

$$\phi = \left(1 - \frac{\rho_s}{\rho_m}\right) (1 - f_V) \quad (3)$$

294 In Equation 3,  $\rho_m$  is the particle density of mineral soil ( $2.65 \text{ g cm}^{-3}$ ),  $\rho_s$  the soil bulk density  
295 ( $\text{g cm}^{-3}$ ) excluding coarse fragments greater than 2 mm (National Ecological Observatory  
296 Network (NEON), 2024c). ~~The term~~ and  $f_V$  is a site-specific value that accounts for the  
297 proportion of soil fragments between 2-20 mm. Soil fragments greater than 20 mm were not  
298 estimated due to limitations in the amount of soil that can be analyzed (National Ecological  
299 Observatory Network (NEON), 2024c). We assume ~~there are no pores within rocks~~ ~~that rock~~  
300 ~~fragments contain no internal pores~~.

301 The ~~second approach to calculate~~ Millington-Quirk model assumes  $\xi$  is ~~the~~ modulated by the  
302 amount of fluid saturation in soil pores (Millington & Shearer, 1971). In contrast, the Marshall

model (Marshall, 1959) ~~, where expresses tortuosity as only a function of porosity ( $\xi = \phi^{1.5}$ )~~, with  $\phi$  defined from Equation 3. ~~The Marshall model is independent of soil water content and assumes tortuosity is only governed by soil structure. The neonSoilFlux package allows users to choose the tortuosity model most appropriate for site-specific conditions and research goals.~~

307

### 308 4.2.3 Soil flux computation

309 We applied Fick's law (Equation 4) to compute the soil flux  $F_{ij}$  ( $\mu\text{mol m}^{-2} \text{s}^{-1}$ ) across two  
310 soil depths  $i$  and  $j$ :

$$F_{ij} = -D_a \frac{dC}{dz} \quad (4)$$

311 where  $D_a$  is the diffusivity ( $\text{m}^2 \text{s}^{-1}$ ) and  $\frac{dC}{dz}$  is the gradient of CO<sub>2</sub> molar concentration ( $\mu\text{mol m}^{-3}$ , so the gradient has units of  $\mu\text{mol m}^{-3} \text{ m}^{-1}$ ). The soil surface flux is theoretically defined  
312 by applying Equation 4 to measurements collected at the soil surface and directly below the  
313 surface. Measurements of soil temperature, soil water content, and soil CO<sub>2</sub> molar concentration  
314 across the soil profile allow for application of Equation 4 across different soil depths. Each site  
315 had three measurement layers, so we denote the flux ~~between which two layers~~ as a three-digit  
316 subscript  $F_{ijk}$  with indicator variables  $i$ ,  $j$ , and  $k$  indicate if a given layer was used (written in  
317 order of increasing depth), according to the following:

- 319 •  $F_{000}$  is a surface flux estimate using the intercept of the linear regression of  $D_a$  with  
320 depth and the slope from the linear regression of CO<sub>2</sub> with depth (which represents  $\frac{dC}{dz}$   
321 in Fick's Law). Tang et al. (2003) used this approach to compute fluxes in an oak-grass  
322 savannah.

- $F_{110}$ ,  $F_{011}$  are fluxes across the two most shallow layers and two deepest layers respectively.
- $F_{101}$  is a surface flux estimate using linear extrapolation using concentration measurements between fluxes estimated at the shallowest and deepest measurement layer. These computed fluxes then form the basis of additional linear extrapolation to the surface. For example, Hirano et al. (2003) and Tang et al. (2005) used an approach similar to  $F_{101}$  in a temperate deciduous broadleaf forest and ponderosa pine forest respectively.

Uncertainty in all  $F_{ijk}$  is computed through quadrature (Taylor, 2022).

### 4.3 Post processing evaluation

Following collection of field measurements and calculation of the soil fluxes from `neonSoilFlux` package, we compared measured  $F_S$  based on closed-dynamic chamber measurements with the LI-COR instruments to a given soil flux calculation from `neonSoilFlux` for each site and flux computation method. Statistics included the associated and quantified the relationship statistically ( $R^2$  value, root mean squared error (RMSE), and signal to noise ratio (SNR), defined as the ratio of a modeled soil flux ( $F_{ijk}$ ) from `neonSoilFlux` to its quadrature uncertainty ( $\sigma_{ijk}$ )).

We observed that the range of values (e.g.  $F_{ijk} \pm \sigma_{ijk}$ ) was much larger than the measured field flux. We evaluated  $|F_S - F_{ijk}| \ll (1 - \epsilon)\sigma_{ijk}$ , where  $F_S$  is a measured field soil flux from the LI-COR 6800 (as the LI-COR 870/8250 was used at only three sites in 2024 but the 6800 was used at all sites in both years). The parameter  $\epsilon$  was an uncertainty reduction factor to

345 evaluate how much the quadrature uncertainty could be reduced while maintaining precision  
346 between modeled  $F_{ijk}$  and measured  $F_S$ ).

347 Finally, for a half-hourly interval we also computed a *post hoc* diffusivity ( $D_a$ ) using the LI-COR  
348 flux along with the CO<sub>2</sub> surface gradient reported by NEON using the measurement levels  
349 closest to the surface.

## 350 5 Results

351 Our overall goal was to design and validate an R package to estimate soil carbon dioxide  
352 fluxes across terrestrial NEON sites using the flux gradient method. Validation of the  
353 approach was based on comparison of estimated fluxes to field measurements made at six  
354 focal sites. We first present our field measurement results, then the concordance between the  
355 modeled and measured results, and lastly assess the factors that influenced the success of the  
356 modeled approach at a given site.

### 357 5.1 Concordance between modelled and measured soil CO<sub>2</sub> flux

### 358 5.2 Field measurements

359 We visited six NEON sites in the summers of 2022 and 2024. Using a closed dynamic chamber  
360 approach, we quantified soil carbon dioxide fluxes over the course of a week at each site. The  
361 sites we visited ranged substantially in both their annual average temperature and precipitation  
362 as well as their biome type (Table 2). These differences also influenced the wide range of observed  
363 flux rates across sites. We used a LI-6800 to take manual hourly measurements at the sites we  
364 visited in 2022 (SRER, SJER, WREF) and half-hourly manual measurements for the sites we  
365 visited in 2024 (UNDE, KONZ, WOOD). In 2024 we also used an automated chamber system

Table 2: Summary of measured soil characteristics and flux results from field measurements across six NEON sites using a LI-COR 6800 (LI-870/8250 measurements omitted to enable direct comparability) via the closed-dynamic chamber method. Numeric values for soil CO<sub>2</sub> flux, soil temperature, and volumetric soil water content (VSWC) are the mean and standard deviation of field measurements at each site.

Site	Flux μmol m <sup>-2</sup> s <sup>-1</sup>	Soil temp °C	VSWC cm <sup>3</sup> cm <sup>-3</sup>	n
UNDE	2.55 ± 0.26	14.33 ± 0.77	0.33 ± 0.02	61
WOOD	3.02 ± 0.4	16.01 ± 1.54	0.28 ± 0.01	53
WREF	3.62 ± 0.3	15.34 ± 1.76	0.27 ± 0.06	21
KONZ	6.35 ± 0.97	27.28 ± 4.14	0.37 ± 0.01	44
SJER	0.94 ± 0.02	41.68 ± 11.22	0.01 ± 0.01	32
SRER	0.72 ± 0.09	47.64 ± 7.46	0.04 ± 0.01	32

366 (LI-870/LI-8250) to take half-hourly measurements 24 hours a day, thereby also capturing  
 367 nighttime fluxes in addition to the daytime fluxes also measured with the LI-6800.

## 368 5.2

369 The timeseries of the measured fluxes from the LI-COR 6800 and 870/8250 were compared  
 370 to modeled soil fluxes from the `neonSoilFlux` R package (Figure 4). We also assessed year-  
 371 long estimated flux time series and compared those to field measurements made at each site  
 372 (Figure 5). Results are reported in local time. Where applicable, sites are displayed from left  
 373 to right by increasing soil temperature (Table 1). Positive values of the flux indicate that there  
 374 is a flux moving towards the surface. Overall, with the exception of SRER (discussed later) the  
 375 computed fluxes determined using a variety of plausible methods spanned the field-measured  
 376 fluxes, but the specific flux-gradient method that best approximated field measurements varied  
 377 by site.

### 378 5.2 Assessment of data gaps

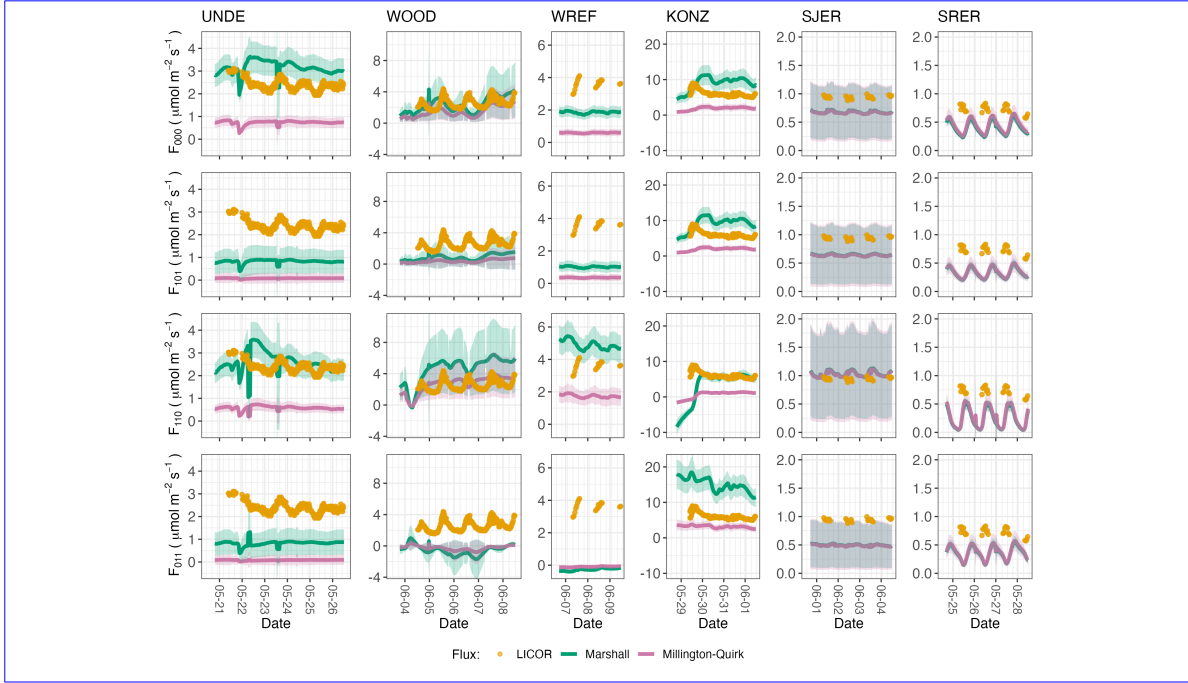


Figure 4: Timeseries of ~~both measured soil surface flux ( $F_s$ ) from field-measured~~ (yellow ~~circles~~~~lines~~) and modeled soil fluxes (green or purple lines) by the `neonSoilFlux` R package. Fluxes from the `neonSoilFlux` R package are separated by the diffusivity model used (Millington-Quirk or Marshall, Section 4.2.2). ~~Vertical Individual vertical axis labels in the first column represent the measurement levels where the flux-gradient approach is applied (Section 4.2.3). Ribbons for modeled soil fluxes represent  $\pm 1$  standard deviation.~~ Results are reported in local time. WREF, SJER, and SRER were sampled in 2022, and UNDE, WOOD, and KONZ were sampled in 2024. Sites (columns) are arranged from left to right in terms of increasing mean annual temperature.

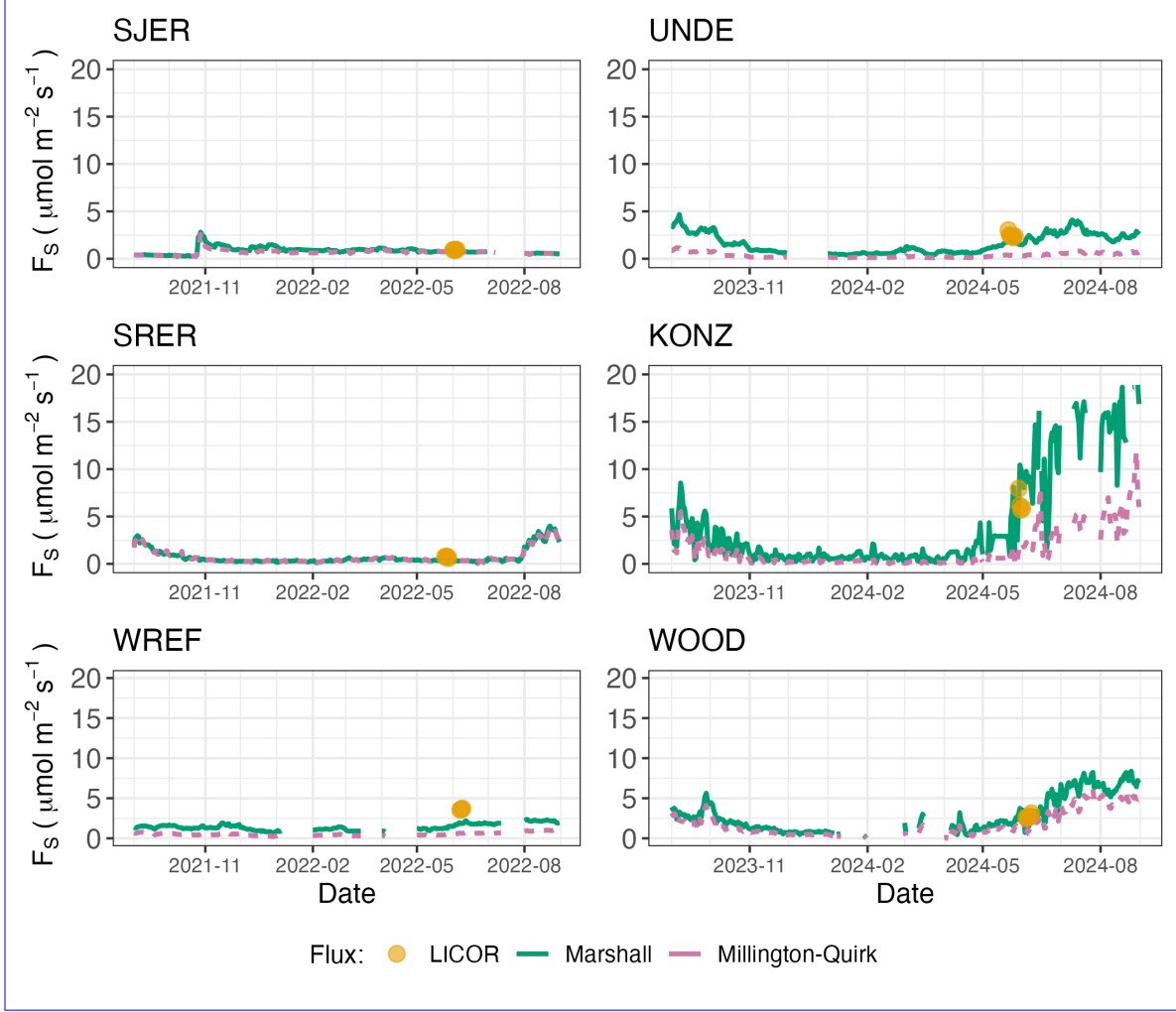


Figure 5: Timeseries of both daily-averaged field  $F_S$  (yellow circles) and daily ensemble averaged soil fluxes (average of  $F_{000}$ ,  $F_{101}$ ,  $F_{011}$ ,  $F_{110}$ , Section 4.2.3) by the `neonSoilFlux` R package, separated by the diffusivity model used (green or purple lines, Millington-Quirk or Marshall, Section 4.2.2).

379 For a given half-hourly time period, the `neonSoilFlux` package assigns a QA flag for  
380 a measurement if more than one values across all measurement depths uses gap-filled data  
381 (Section 4.2.1). Panel a of Figure ?? reports the proportion of gap-filled data for all input  
382 environmental measurements at each site during the period when field measurements were  
383 made. Soil fluxes are computed from 4 different types of input measurements ( $T_S$ ,  $SWC$ ,  $P$ ,  
384 and  $CO_2$ ), any of which could have a QA flag in a half-hourly interval. Panel b of Figure ??  
385 displays at each site the distribution of the number of different gap-filled measurements used  
386 to compute a half-hourly flux. The largest cause of measurements needing to be gap-filled  
387 was missing or flagged soil moisture data. Calculating fluxes for WOOD and SJER required  
388 using the largest proportion of gap-filled measurements, due to substantially large fractions  
389 of flagged or missing  $SWC$  and  $T_S$  data.

390 Panel a) Proportion of input gap-filled environmental measurements used to generate  $F_S$  from  
391 the `neonSoilFlux` package, by study site. Panel b) distribution of the usage of gap-filled  
392 measurements at each site.

## 393 5.2 Assessing the signal to noise ratio (SNR) and evaluating estimated 394 uncertainties

395 The computed signal to noise ratio (SNR) and the proportion of measured field fluxes within  
396 the modeled uncertainty for a given flux computation method  $F_{ijk}$  suggest that there was  
397 substantial variability in the agreement between the gradient method and field-measured  
398 observations (Figure ??, Section 4.3). Here, values of SNR greater than unity indicate  
399 lower reported uncertainty, as propagated by quadrature due to a relatively higher precision  
400 of measured input variables ( $CO_2$ ,  $T_S$ ,  $SWC$ , or  $P$ ). We calculated a statistical relationship  
401 between the various estimates of soil flux computed by `neonSoilFlux` and the field-measured

402 fluxes within daily interval periods. Statistics for these comparisons are reported in Figure 6,  
403 which also shows how these fall relative to a 1:1 line.

404 The sensitivity to an uncertainty reduction factor ( $\epsilon$ , bottom panels in Figure ??) demonstrates  
405 how concordance between measured and modeled fluxes would be affected if environmental  
406 measurement uncertainty  $\sigma_{ijk}$  were to decrease. As  $\epsilon$  increases from left to right in each figure,  
407 the possible range of values for each predicted flux value decreases and the proportion of  
408 measured fluxes that fall within that range also decreases.

## 409 5.2 Effects of method choice on diffusivity estimates

410 We assessed the distribution of  $D_a$  (from both the Marshall and Millington-Quirk methods)  
411 at each study site, and also computed a *post hoc* estimate of  $D_a$  using field surface flux  
412 measurements (Section 4.2.2). For the field-estimated measurements we omitted negative  
413 values of  $D_a$ , as that indicates the CO<sub>2</sub> gradient decreases with soil depth (thereby violating  
414 assumptions of the flux-gradient method, which is our focus here). In four of six field sites, the  
415 *post hoc*  $D_a$  estimate fell roughly between the two diffusion estimation methods; however this  
416 was less the case in the two driest sites, SJER and SRER (Table 1), where the field estimate of  
417 diffusivity was either lower or higher than both of the other methods (Figure 7).

## 418 6 Discussion

419 This study presents a unified data science workflow to efficiently process automated measure-  
420 ments of belowground soil CO<sub>2</sub> concentrations, soil water content, and soil temperature to  
421 infer estimates of soil surface CO<sub>2</sub> effluxes through application of Fick's Law (Equation 4).  
422 Our core goals in this study were: (1) to generate estimates of soil flux from continuous soil

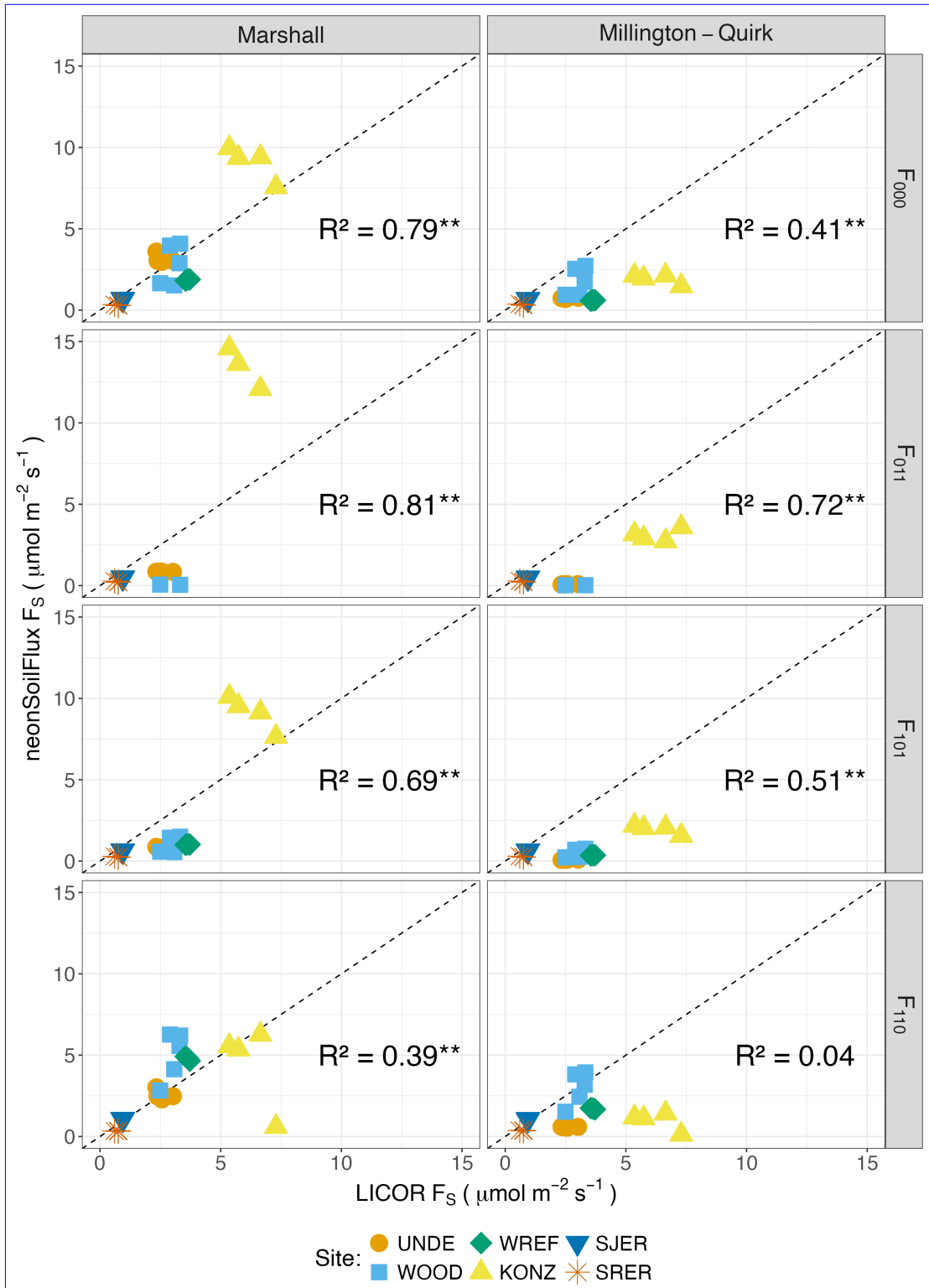


Figure 6: Top panels: distribution of SNR values across Statistical comparison between measured fluxes at each of NEON site with fluxes reported by neonSoilFlux with the different sites for modeled efflux flux calculation approaches and diffusivity calculations applied. Points are daily averages and LICOR  $F_S$  values are from the neonSoilFlux package instrument only, depending on for consistency. The dotted line represents a 1:1 relationship, and the diffusivity calculation used (Millington-Quirk or Marshall) reported  $R^2$  quantifies the relationship between field-measured and neonSoilFlux estimated fluxes. \* = significance at the 5% level, Section 4.2.2)\*\* = significance at the 1% level. Bottom panels: Proportion-The low-value outlier from KONZ in the  $F_{110}$  Marshall plot is an example of measured

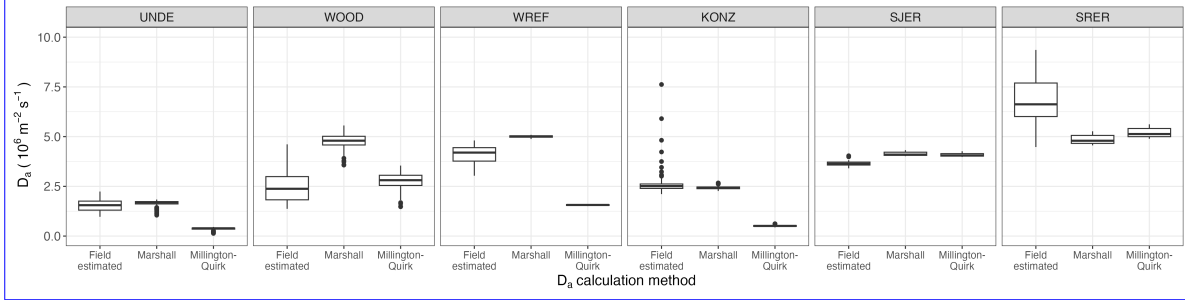


Figure 7: Distribution of diffusivity ( $D_a$ ) at each study site. Values of  $D_a$  were provided by the `neonSoilFlux` package, computed from the Millington-Quirk or Marshall models (Section 4.2.2). A post-hoc estimate of diffusivity (labeled as “Field estimated”) was computed through the field measured flux (Figure 4), divided by the CO<sub>2</sub> gradient from the measurement levels closest to the soil surface, as reported by NEON. We only used  $F_S$  measured by the LICOR 6800 at all sites to standardize comparisons.

423 sensor data at terrestrial NEON sites using the flux-gradient method and then (2) to compare  
 424 those estimates to field-measured fluxes based on the closed chamber approach at six NEON  
 425 focal sites. We discuss our progress toward these core goals through (1) an overall evaluation  
 426 of the flux-gradient approach (and uncertainty calculation) and (2) site-specific evaluation of  
 427 differences in estimated vs measured fluxes.

## 428 6.1 General evaluation of flux-gradient approach

429 Key assumptions of the flux-gradient approach are that CO<sub>2</sub> concentrations increase through-  
 430 out the soil profile such that the highest concentrations are observed in the deepest lay-  
 431 ers. Additionally, field flux measurements should correlate with  $F_{000}$  because they represent  
 432 surface fluxes. Periods where this gradient condition are not met generally are connected  
 433 to processes that occur during soil wetting events, where more shallow soil layers produce  
 434 higher concentrations of CO<sub>2</sub> due to microbial respiration pulses following rewetting. This  
 435 effect is likely to be largest at sites with rich organic soils (e.g. KONZ). Based on this  
 436 reasoning, in these types of situations we would *a priori* expect  $F_{011} \leq F_{101} \leq F_{110} \leq F_{000}$

<sup>437</sup>  $F_{011}$  (deepest layers)  $\leq F_{101} \leq F_{110}$  (shallow layers)  $\leq F_{000}$  (all layers) because the previous  
<sup>438</sup> flux estimates rely primarily on CO<sub>2</sub> concentrations at deeper depths, and could miss high  
<sup>439</sup> concentrations of CO<sub>2</sub> produced in shallower layers.

<sup>440</sup> When modeling soil respiration, typically a non-linear response function that also considers  
<sup>441</sup> soil type is used (Bouma & Bryla, 2000; Yan et al., 2016, 2018). For the `neonSoilFlux`  
<sup>442</sup> package, soil type is connected to the measurement of bulk density, which was characterized  
<sup>443</sup> at each NEON site. This bulk density estimate is based on replicate samples collected from  
<sup>444</sup> the site megapit at a subset of soil horizons, with an estimated uncertainty of  $\pm 5\%$  (National  
<sup>445</sup> Ecological Observatory Network (NEON), 2024c). Coarse fragment estimates also have very  
<sup>446</sup> large uncertainties, but because the volume fraction tends to be low in surface soils it ~~probably~~  
<sup>447</sup> ~~wouldn't is unlikely to~~ contribute much additional flux uncertainty.

<sup>448</sup> Our results suggest that the most important way to improve reliability of the flux estimate is  
<sup>449</sup> to reduce the usage of gap-filled data. The current approach to gap filling in `neonSoilFlux`  
<sup>450</sup> uses monthly mean data to gap fill—this approach decreases the ability of the estimate to  
<sup>451</sup> be responsive to ~~short turn-~~short-term pulses that occur with rapid weather shifts. Four sites  
<sup>452</sup> (KONZ, SRER, WREF, and UNDE) had more than 75% of half-hourly periods with no-gap  
<sup>453</sup> filled measurements ([Figure S1, Supplementary Information](#)). Two sites (SJER and WOOD)  
<sup>454</sup> had more than 75% of half-hourly intervals with just one gap-filled measurement. The large  
<sup>455</sup> uncertainty evident in Figure 4 for estimates from WOOD and SJER are thus due in part  
<sup>456</sup> to the gap-filling used in these sites (Figure S1). While we did not need to use gap-filled  
<sup>457</sup> measurements to compute the flux at WREF, field data collection occurred following a severe  
<sup>458</sup> rainstorm, with soils at the beginning of the sampling week near their water holding capacity.  
<sup>459</sup> ~~We~~ In general, we recommend that whenever possible, knowledge of local field conditions should  
<sup>460</sup> influence analysis decisions in addition to any QA filtering protocols in the `neonSoilFlux`  
<sup>461</sup> package.

We recognize that this gap-filling approach may lead to gap-filled values that are quite different from the actual values, such as an underestimate of soil moisture following rain events. Further extensions of the gap filling method could use more sophisticated gap-filling routines, similar to what is used for net ecosystem carbon exchange (Falge et al., 2001; Liu et al., 2023; Mariethoz et al., 2015; Moffat et al., 2007; Zhang et al., 2023). Additionally, since the deepest temperature and soil moisture sensors are located below the deepest CO<sub>2</sub> sensors at NEON sites, it is possible that excluding these deeper layers from consideration prior to analysis would lead to a reduced need for gap filling. Future iterations of the neonSoilFlux package may incorporate this as an option. The current gap-filling routine provides a consistent approach that can be applied to each data stream, but further work may explore alternative gap-filling approaches.

## 6.2 Evaluation of flux-gradient approach at each site

Derived results from the neonSoilFlux package have patterns that are broadly consistent with those directly measured in the field (Figure 4 and Figure 5), even though statistical comparisons between the field-measured and neonSoilFlux values were quite variable (e.g. R<sup>2</sup> ranging from 0.04 to 0.81; Figure 6). One advantage of the neonSoilFlux package is its ability to calculate fluxes across different soil depths (Figure 3), which allows for additional site-specific customization. We believe the package can provide a useful baseline estimate of soil fluxes that can always be complemented through additional field measurements.

The six locations studied provide a range of case studies that suggest different considerations may apply to different sites when applying the flux-gradient method. For example, the Santa Rita Experimental Range (SRER) is a desert site characterized by sandy soil, which also was the location of the highest field soil temperatures that we observed (Table 2). At SRER the flux across the top two layers ( $F_{110}$ ) produced a pattern of soil flux most consistent with the observed field data. The remaining methods  $F_{101}$ ,  $F_{011}$ , or  $F_{000}$  are derived from information

486 taken from the deepest layer, which seems to have been decoupled from the surface layers both  
487 in terms of temperature and CO<sub>2</sub> concentration. This may be a general circumstance where  
488 there are large diurnal temperature extremes that rapidly change during the course of a day  
489 and overnight, leading to lags in the timing of when temperature increases propagate down to  
490 deeper soil layers.

491 Immediately prior to our visit to Konza Prairie (KONZ), that site that experienced a significant  
492 rain event that led to wet soils that gradually dried out over the course of our time there.  
493 This pulse of precipitation increased the soil CO<sub>2</sub> concentration at the top layer above the  
494 concentrations in lower layers, leading to negative estimated flux values at the start of the  
495 ~~experiment~~field sampling period. In this case it was only when the soil began to return to a  
496 baseline level that the assumptions of the flux-gradient method were again met.

497 ~~Thus, when Both of the previous cases also provide context for the variable statistical~~  
498 ~~comparisons between field-measured soil fluxes and neonSoilFlux outputs (Figure 6). When~~  
499 ~~considering systematic deployment of this method across a measurement network, there~~  
500 ~~are a number of independent challenges that require careful consideration. There are clear~~  
501 ~~tradeoffs between (1) accuracy of modeled fluxes (defined here as closeness to field-measured~~  
502 ~~F<sub>S</sub> and the uncertainty reduction factor  $\epsilon$ ), (2) precision (~~which could be~~ defined by the~~  
503 ~~SNR~~signal to noise ratio~~~~, and (3) the choice of the diffusivity model (Section 4.2.2) or flux  
504 ~~computation method (Section 4.2.3)~~used (Figure ??)~~. There was no predictable pattern in~~  
505 ~~SNR for either the flux computation method or diffusivity calculation, indicating that output~~  
506 ~~uncertainty is driven primarily by input~~. A sensitivity analysis (Figure S2, Supplemental  
507 ~~Information) found that flux output uncertainty was dominated by~~ measurement uncertainty  
508 ~~(T<sub>S</sub>, P, SWC, or CO<sub>2</sub>) — Across the different flux computation methods, the proportion~~  
509 ~~of measured fluxes where |F<sub>S</sub> — F<sub>ijk</sub>| < (1 —  $\epsilon$ )σ<sub>ijk</sub> decreased as  $\epsilon$  increased, except where~~  
510 ~~field F<sub>S</sub> was already outside of the modeled range (i.e. UNDE and WREF). The method~~

511 rather than by the diffusivity method used to compute soil flux. Notably, the  $F_{110}$  (where  
512 soil flux was computed from the top two soil layers) was the method was least sensitive to  
513 the uncertainty reduction factor ( $\epsilon$ ). This lack of sensitivity could represent that a surface  
514 chamber-based measurement method (e.g. with a LI-COR instrument) measures the flux up  
515 out of the surface layer and thus is most closely related to assumptions and measurements  
516 inherent in the  $F_{110}$  method measurement uncertainty likely because it best aligns with the  
517 surface chamber measurement assumptions.

518 Finally, comparing the effects of different diffusivity estimation methods on the match between  
519 modeled and measured fluxes (Figure 5) highlights the sensitivity of  $F_{ijk}$  to diffusivity. The  
520 comparison between diffusivity estimates compared to field estimated diffusivity (Figure 7)  
521 demonstrates that site parameters can dictate which measure of diffusivity is most likely to be  
522 accurate in a given environmental context. Site-specific differences ~~a-are~~ largely a reflection of  
523 differences in soil moisture across the sites (Table 1), as not all diffusivity estimation methods  
524 incorporate soil moisture equivalently. While we here have compares two approaches to calculate  
525 diffusivity (the Millington-Quirk and Marshall models), it may be valuable to evaluate other  
526 diffusivity models (e.g. the Moldrup model; Moldrup et al. (1999)) as well. Ultimately the  
527 choice of a particular diffusivity model could be determined based on knowledge of site-specific  
528 evaluations or a set of these models could be used to generate a model ensemble average as a  
529 means to trade precision for a more general approach.

### 530 6.3 Recommendations for future method development

531 The `neonSoilFlux` package provides ~~three different several~~ approaches to estimate soil flux  
532 using the gradient method. We believe these approaches enable the software to be used across  
533 a range of site-specific assumptions (Maier & Schack-Kirchner, 2014). We note, however, that  
534 this choice can have a determinative approach on the calculated values. Ensemble averaging

535 approaches (Elshall et al., 2018; Raftery et al., 2005) may be one way to address this problem if  
536 the goal is to calculate fluxes using the same method at a diverse range of different sites. Two  
537 other ideas would be to apply machine learning algorithms (e.g. random ~~trees~~forest) to generate  
538 a single flux estimate across diverse sites, or using co-located estimates of net ecosystem carbon  
539 exchange from eddy-flux towers to further constrain results or to assess soil flux results for  
540 plausibility ~~–(Phillips et al., 2017).~~

541 These challenges notwithstanding, the method used here and made available in the  
542 `neonSoilFlux` R package has the potential to produce nearly continuous estimates of flux  
543 across all terrestrial NEON sites. These estimates are a significant improvement on available  
544 approaches to constrain the portion of ecosystem respiration attributable to the soil. This, in  
545 turn, also aids in our ability to understand the soil contribution to the net ecosystem flux  
546 measured at these sites using the co-located eddy flux towers.

## 547 7 Conclusions

548 We ~~have here presented an~~used the R package `neonSoilFlux` ~~for the estimation of soil CO<sub>2</sub>~~  
549 ~~fluxes from continuous buried soil sensor measurements across terrestrial National Ecological~~  
550 ~~Observatory Network~~to estimate soil CO<sub>2</sub> fluxes with the flux-gradient method using data  
551 from buried soil sensors at NEON terrestrial sites. We compared the predicted fluxes to those  
552 measured directly using a field-based closed chamber approach. ~~We find that the flux gradient~~  
553 ~~method, while~~Soil fluxes from `neonSoilFlux` were broadly effective at producing estimates of  
554 flux comparable to those measured in the field using a chamber-based technique~~, is~~. However  
555 neonSoilFlux outputs are quite sensitive to a number of issues, including~~most prominently~~:  
556 missing data (and thus gap-filling of input measurement datasets), the selection of soil depths  
557 used to best calculate the gradient (which may vary between sites), and finally the choice of

558 method used for estimating soil diffusivity. Despite these challenges, the broad geographic scale  
559 and high temporal resolution of the NEON data make a compelling case for continued efforts to  
560 refine this approach to help us understand how. The flexibility of the `neonSoilFlux` package  
561 allows the user to evaluate each of these issues with site-specific knowledge and contexts.  
562 Future refinements and subsequent validation of `neonSoilFlux` outputs will feed forward into  
563 evaluating soil carbon fluxes broader spatial scales to enhance understanding of the ways in  
564 which soils across diverse ecosystems are responding to a changing climate.

## 565 Sources Cited

- 566 Ayres, E., Reichle, R. H., Colliander, A., Cosh, M. H., & Smith, L. (2024). Validation of  
567 Remotely Sensed and Modeled Soil Moisture at Forested and Unforested NEON Sites.  
568 *IEEE Journal of Selected Topics in Applied Earth Observations and Remote Sensing*, 17,  
569 14248–14264. <https://doi.org/10.1109/JSTARS.2024.3430928>
- 570 Baldocchi, D. (2014). Measuring fluxes of trace gases and energy between ecosystems and the  
571 atmosphere - the state and future of the eddy covariance method. *Global Change Biology*,  
572 20(12), 3600–3609. <https://doi.org/10.1111/gcb.12649>
- 573 Berenbaum, M. R., Carpenter, S. R., Hampton, S. E., Running, S. W., & Stanzione, D. C.  
574 (2015). Report from the NSF BIO Advisory Committee Subcommittee on NEON Scope  
575 Impacts.
- 576 Bond-Lamberty, B. (2018). New Techniques and Data for Understanding the Global Soil  
577 Respiration Flux. *Earth's Future*, 6(9), 1176–1180. <https://doi.org/10.1029/2018EF000866>
- 578 Bond-Lamberty, B., Ballantyne, A., Berryman, E., Fluet-Chouinard, E., Jian, J., Morris, K.  
579 A., Rey, A., & Vargas, R. (2024). Twenty Years of Progress, Challenges, and Opportuni-  
580 ties in Measuring and Understanding Soil Respiration. *Journal of Geophysical Research: Biogeosciences*, 129(2), e2023JG007637. <https://doi.org/10.1029/2023JG007637>

- 582 Bond-Lamberty, B., Christianson, D. S., Malhotra, A., Pennington, S. C., Sihi, D., AghaK-  
583 ouchak, A., Anjileli, H., Altaf Arain, M., Armesto, J. J., Ashraf, S., Ataka, M., Baldocchi,  
584 D., Andrew Black, T., Buchmann, N., Carbone, M. S., Chang, S.-C., Crill, P., Curtis, P.  
585 S., Davidson, E. A., ... Zou, J. (2020). COSORE: A community database for continuous  
586 soil respiration and other soil-atmosphere greenhouse gas flux data. *Global Change Biology*,  
587 26(12), 7268–7283. <https://doi.org/10.1111/gcb.15353>
- 588 Bond-Lamberty, B., & Thomson, A. (2010). A global database of soil respiration data.  
589 *Biogeosciences*, 7(6), 1915–1926. <https://doi.org/10.5194/bg-7-1915-2010>
- 590 Bond-Lamberty, B., Wang, C., & Gower, S. T. (2004). A global relationship between the  
591 heterotrophic and autotrophic components of soil respiration? *Global Change Biology*,  
592 10(10), 1756–1766. <https://doi.org/10.1111/j.1365-2486.2004.00816.x>
- 593 Bouma, T. J., & Bryla, D. R. (2000). On the assessment of root and soil respiration for soils of  
594 different textures: Interactions with soil moisture contents and soil CO<sub>2</sub> concentrations.  
595 *Plant and Soil*, 227(1), 215–221. <https://doi.org/10.1023/A:1026502414977>
- 596 Chen, H., & Tian, H.-Q. (2005). Does a General Temperature-Dependent Q10 Model of Soil  
597 Respiration Exist at Biome and Global Scale? *Journal of Integrative Plant Biology*, 47(11),  
598 1288–1302. <https://doi.org/10.1111/j.1744-7909.2005.00211.x>
- 599 Davidson, E. A., Janssens, I. A., & Luo, Y. (2006). On the variability of respiration in  
600 terrestrial ecosystems: Moving beyond Q10. *Global Change Biology*, 12, 154–164. <https://doi.org/10.1111/j.1365-2486.2005.01065.x>
- 602 Desai, A. R., Murphy, B. A., Wiesner, S., Thom, J., Butterworth, B. J., Koupaei-Abyazani, N.,  
603 Muttaqin, A., Paleri, S., Talib, A., Turner, J., Mineau, J., Merrelli, A., Stoy, P., & Davis,  
604 K. (2022). Drivers of Decadal Carbon Fluxes Across Temperate Ecosystems. *Journal of  
605 Geophysical Research: Biogeosciences*, 127(12), e2022JG007014. <https://doi.org/10.1029/2022JG007014>
- 607 Efron, B., & Tibshirani, R. J. (1994). *An Introduction to the Bootstrap*. Chapman and

- 608 Hall/CRC. <https://doi.org/10.1201/9780429246593>
- 609 Elshall, A. S., Ye, M., Pei, Y., Zhang, F., Niu, G.-Y., & Barron-Gafford, G. A. (2018). Relative  
610 model score: A scoring rule for evaluating ensemble simulations with application to microbial  
611 soil respiration modeling. *Stochastic Environmental Research and Risk Assessment*, 32(10),  
612 2809–2819. <https://doi.org/10.1007/s00477-018-1592-3>
- 613 Falge, E., Baldocchi, D., Olson, R., Anthoni, P., Aubinet, M., Bernhofer, C., Burba, G.,  
614 Ceulemans, R., Clement, R., Dolman, H., Granier, A., Gross, P., Grünwald, T., Hollinger,  
615 D., Jensen, N.-O., Katul, G., Keronen, P., Kowalski, A., Lai, C. T., ... Wofsy, S. (2001).  
616 Gap filling strategies for defensible annual sums of net ecosystem exchange. *Agricultural  
617 and Forest Meteorology*, 107(1), 43–69. [https://doi.org/10.1016/S0168-1923\(00\)00225-2](https://doi.org/10.1016/S0168-1923(00)00225-2)
- 618 Farrance, I., & Frenkel, R. (2012). *Uncertainty of Measurement: A Review of the Rules  
619 for Calculating Uncertainty Components through Functional Relationships*. *The Clinical  
620 Biochemist Reviews*, 33(2), 49–75.
- 621
- 622 Friedlingstein, P., O'Sullivan, M., Jones, M. W., Andrew, R. M., ~~Bakker, D. C. E.~~, Hauck, J.,  
623 Landschützer, P., Le Quéré, C., ~~Li, H.~~ Luijkx, I. T., ~~Olsen, A.~~, Peters, G. P., Peters, W.,  
624 Pongratz, J., Schwingshackl, C., Sitch, S., Canadell, J. G., Ciais, P., Jackson, R. B., Alin, S.  
625 R., ~~Anthoni, P., ... Zheng, B. (2023... Zeng, J. (2025)~~. Global Carbon Budget 2023–2024.  
626 *Earth System Science Data*, ~~-5301-5369-~~17(3), ~~965-1039~~. <https://doi.org/10.5194/essd-17-965-2025>
- 627
- 628 Hamdi, S., Moyano, F., Sall, S., Bernoux, M., & Chevallier, T. (2013). Synthesis analysis  
629 of the temperature sensitivity of soil respiration from laboratory studies in relation to  
630 incubation methods and soil conditions. *Soil Biology and Biochemistry*, 58, 115–126.  
631 <https://doi.org/10.1016/j.soilbio.2012.11.012>
- 632
- 633 Hirano, T., Kim, H., & Tanaka, Y. (2003). Long-term half-hourly measurement of soil CO<sub>2</sub>

- 634 concentration and soil respiration in a temperate deciduous forest. *Journal of Geophysical*  
635 *Research: Atmospheres*, 108(D20). <https://doi.org/10.1029/2003JD003766>
- 636 Jackson, R. B., Lajtha, K., Crow, S. E., Hugelius, G., Kramer, M. G., & Piñeiro, G. (2017).  
637 The Ecology of Soil Carbon: Pools, Vulnerabilities, and Biotic and Abiotic Controls.  
638 *Annual Review of Ecology, Evolution and Systematics*, 48(Volume 48, 2017), 419–445.  
639 <https://doi.org/10.1146/annurev-ecolsys-112414-054234>
- 640 Jian, J., Bailey, V., Dorheim, K., Konings, A. G., Hao, D., Shiklomanov, A. N., Snyder,  
641 A., Steele, M., Teramoto, M., Vargas, R., & Bond-Lamberty, B. (2022). Historically  
642 inconsistent productivity and respiration fluxes in the global terrestrial carbon cycle. *Nature*  
643 *Communications*, 13(1), 1733. <https://doi.org/10.1038/s41467-022-29391-5>
- 644 Jian, J., Vargas, R., Anderson-Teixeira, K., Stell, E., Herrmann, V., Horn, M., Kholod, N.,  
645 Manzon, J., Marchesi, R., Paredes, D., & Bond-Lamberty, B. (2021). A restructured and  
646 updated global soil respiration database (SRDB-V5). *Earth System Science Data*, 13(2),  
647 255–267. <https://doi.org/10.5194/essd-13-255-2021>
- 648 Jiang, J., Feng, L., Hu, J., Liu, H., Zhu, C., Chen, B., & Chen, T. (2024). Global soil  
649 respiration predictions with associated uncertainties from different spatio-temporal data  
650 subsets. *Ecological Informatics*, 82, 102777. <https://doi.org/10.1016/j.ecoinf.2024.102777>
- 651 Jobbágy, E. G., & Jackson, R. B. (2000). The Vertical Distribution of Soil Organic Carbon  
652 and its Relation to Climate and Vegetation. *Ecological Applications*, 10(2), 423–436.  
653 [https://doi.org/10.1890/1051-0761\(2000\)010%5B0423:TVDOSO%5D2.0.CO;2](https://doi.org/10.1890/1051-0761(2000)010%5B0423:TVDOSO%5D2.0.CO;2)
- 654 Liu, K., Li, X., Wang, S., & Zhang, H. (2023). A robust gap-filling approach for European  
655 Space Agency Climate Change Initiative (ESA CCI) soil moisture integrating satellite  
656 observations, model-driven knowledge, and spatiotemporal machine learning. *Hydrology*  
657 and *Earth System Sciences*, 27(2), 577–598. <https://doi.org/10.5194/hess-27-577-2023>
- 658 Lunch, C., Laney, C., Mietkiewicz, N., Sokol, E., Cawley, K., & NEON (National Ecological  
659 Observatory Network). (2025). *neonUtilities: Utilities for working with NEON data*. <https://>

- 660        [//doi.org/10.32614/CRAN.package.neonUtilities](https://doi.org/10.32614/CRAN.package.neonUtilities)
- 661    Luo, Y., Ogle, K., Tucker, C., Fei, S., Gao, C., LaDeau, S., Clark, J. S., & Schimel, D. S. (2011).  
662        Ecological forecasting and data assimilation in a data-rich era. *Ecological Applications*,  
663        21(5), 1429–1442. <https://doi.org/10.1890/09-1275.1>
- 664    Maier, M., & Schack-Kirchner, H. (2014). Using the gradient method to determine soil gas  
665        flux: A review. *Agricultural and Forest Meteorology*, 192–193, 78–95. <https://doi.org/10.1016/j.agrformet.2014.03.006>
- 666    Mariethoz, G., Linde, N., Jougnot, D., & Rezaee, H. (2015). Feature-preserving interpolation  
667        and filtering of environmental time series. *Environmental Modelling & Software*, 72, 71–76.  
668        <https://doi.org/10.1016/j.envsoft.2015.07.001>
- 669    Marshall, T. J. (1959). The Diffusion of Gases Through Porous Media. *Journal of Soil Science*,  
670        10(1), 79–82. <https://doi.org/10.1111/j.1365-2389.1959.tb00667.x>
- 671    Millington, R. J., & Shearer, R. C. (1971). Diffusion in aggregated porous media. *Soil Science*,  
672        111(6), 372–378.
- 673    Moffat, A. M., Papale, D., Reichstein, M., Hollinger, D. Y., Richardson, A. D., Barr, A. G.,  
674        Beckstein, C., Braswell, B. H., Churkina, G., Desai, A. R., Falge, E., Gove, J. H., Heimann,  
675        M., Hui, D., Jarvis, A. J., Kattge, J., Noormets, A., & Stauch, V. J. (2007). Comprehensive  
676        comparison of gap-filling techniques for eddy covariance net carbon fluxes. *Agricultural and  
677        Forest Meteorology*, 147(3), 209–232. <https://doi.org/10.1016/j.agrformet.2007.08.011>
- 678    Moldrup, P., Olesen, T., Yamaguchi, T., Schjønning, P., & Rolston, D. E. (1999). Modeling  
679        diffusion and reaction in soils: 9. The Buckingham-Burdine-Campbell equation for gas  
680        diffusivity in undisturbed soil. *Soil Science*, 164(2), 75.
- 681    National Ecological Observatory Network (NEON). (2024a). *Barometric pressure*  
682        (*DP1.00004.001*). National Ecological Observatory Network (NEON). <https://doi.org/10.48443/RT4V-KZ04>
- 683    National Ecological Observatory Network (NEON). (2024b). *Soil CO2 concen-*

- 686 *tration (DP1.00095.001)*. National Ecological Observatory Network (NEON).  
687 <https://doi.org/10.48443/E7GR-6G94>
- 688 National Ecological Observatory Network (NEON). (2024c). *Soil physical and chemical prop-*  
689 *erties, Megapit (DP1.00096.001)*. National Ecological Observatory Network (NEON).  
690 <https://doi.org/10.48443/S6ND-Q840>
- 691 National Ecological Observatory Network (NEON). (2024d). *Soil temperature (DP1.00041.001)*.  
692 National Ecological Observatory Network (NEON). <https://doi.org/10.48443/Q24X-PW21>
- 693 National Ecological Observatory Network (NEON). (2024e). *Soil water content and water*  
694 *salinity (DP1.00094.001)*. National Ecological Observatory Network (NEON). <https://doi.>  
695 <https://doi.org/10.48443/A8VY-Y813>
- 696 Norman, J. M., Kucharik, C. J., Gower, S. T., Baldocchi, D. D., Crill, P. M., Rayment,  
697 M., Savage, K., & Striegl, R. G. (1997). A comparison of six methods for measuring  
698 soil-surface carbon dioxide fluxes. *Journal of Geophysical Research: Atmospheres*, 102(D24),  
699 28771–28777. <https://doi.org/10.1029/97JD01440>
- 700 Phillips, C. L., Bond-Lamberty, B., Desai, A. R., Lavoie, M., Risk, D., Tang, J., Todd-Brown,  
701 K., & Vargas, R. (2017). The value of soil respiration measurements for interpreting and  
702 modeling terrestrial carbon cycling. *Plant and Soil*, 413(1), 1–25. <https://doi.org/10.1007/s11104-016-3084-x>
- 703 Raftery, A. E., Gneiting, T., Balabdaoui, F., & Polakowski, M. (2005). *Using Bayesian Model*  
704 *Averaging to Calibrate Forecast Ensembles*. <https://doi.org/10.1175/MWR2906.1>
- 705 Sallam, A., Jury, W. A., & Letey, J. (1984). Measurement of Gas Diffusion Coefficient under  
706 Relatively Low Air-filled Porosity. *Soil Science Society of America Journal*, 48(1), 3–6.  
707 <https://doi.org/10.2136/sssaj1984.03615995004800010001x>
- 708 Shao, J., Zhou, X., Luo, Y., Li, B., Aurela, M., Billesbach, D., Blanken, P. D., Bracho, R.,  
709 Chen, J., Fischer, M., Fu, Y., Gu, L., Han, S., He, Y., Kolb, T., Li, Y., Nagy, Z., Niu, S.,  
710 Oechel, W. C., ... Zhang, J. (2015). Biotic and climatic controls on interannual variability

- 712 in carbon fluxes across terrestrial ecosystems. *Agricultural and Forest Meteorology*, 205,  
713 11–22. <https://doi.org/10.1016/j.agrformet.2015.02.007>
- 714 Shao, P., Zeng, X., Moore, D. J. P., & Zeng, X. (2013). Soil microbial respiration from  
715 observations and Earth System Models. *Environmental Research Letters*, 8(3), 034034.  
716 <https://doi.org/10.1088/1748-9326/8/3/034034>
- 717 Sihi, D., Gerber, S., Inglett, P. W., & Inglett, K. S. (2016). Comparing models of microbial–  
718 substrate interactions and their response to warming. *Biogeosciences*, 13(6), 1733–1752.  
719 <https://doi.org/10.5194/bg-13-1733-2016>
- 720 Tang, J., Baldocchi, D. D., Qi, Y., & Xu, L. (2003). Assessing soil CO<sub>2</sub> efflux using continuous  
721 measurements of CO<sub>2</sub> profiles in soils with small solid-state sensors. *Agricultural and Forest  
722 Meteorology*, 118(3), 207–220. [https://doi.org/10.1016/S0168-1923\(03\)00112-6](https://doi.org/10.1016/S0168-1923(03)00112-6)
- 723 Tang, J., Misson, L., Gershenson, A., Cheng, W., & Goldstein, A. H. (2005). Continuous  
724 measurements of soil respiration with and without roots in a ponderosa pine plantation  
725 in the Sierra Nevada Mountains. *Agricultural and Forest Meteorology*, 132(3), 212–227.  
726 <https://doi.org/10.1016/j.agrformet.2005.07.011>
- 727 Taylor, J. R. (2022). *An Introduction to Error Analysis: The Study of Uncertainties in Physical  
728 Measurements, Third Edition* (3rd ed.). University Science Press.
- 729 Yan, Z., Bond-Lamberty, B., Todd-Brown, K. E., Bailey, V. L., Li, S., Liu, C., & Liu, C. (2018).  
730 A moisture function of soil heterotrophic respiration that incorporates microscale processes.  
731 *Nature Communications*, 9(1), 2562. <https://doi.org/10.1038/s41467-018-04971-6>
- 732 Yan, Z., Liu, C., Todd-Brown, K. E., Liu, Y., Bond-Lamberty, B., & Bailey, V. L. (2016).  
733 Pore-scale investigation on the response of heterotrophic respiration to moisture conditions  
734 in heterogeneous soils. *Biogeochemistry*, 131(1), 121–134. <https://doi.org/10.1007/s10533-016-0270-0>
- 735 Zhang, R., Kim, S., Kim, H., Fang, B., Sharma, A., & Lakshmi, V. (2023). Temporal Gap-Filling  
736 of 12-Hourly SMAP Soil Moisture Over the CONUS Using Water Balance Budgeting. *Water*

738        *Resources Research*, 59(12), e2023WR034457. <https://doi.org/10.1029/2023WR034457>

739        Zobitz, J., Ayres, E., O'Rourke, K., Werbin, Z., Lee, L., Abdi, R., Mehmeti, D., & Xiong, L.

740        (2024). *neonSoilFlux: Compute Soil Carbon Fluxes for the National Ecological Observatory*

741        *Network Sites*. <https://doi.org/10.32614/CRAN.package.neonSoilFlux>